Targeted nuclear irradiation with a proton microbeam induces oxidative DNA base damage and triggers the recruitment of DNA glycosylases OGG1 and NTH1

Elena Robeska, Kevin Lalanne, François Vianna-Legros, Haser Hasan Sutcu, Andriy Khobta, Didier Busso, J. Pablo Radicella, Anna Campalans, Céline Baldeyron

Targeted nuclear irradiation with a proton microbeam induces oxidative DNA base damage and triggers the recruitment of DNA glycosylases OGG1 and NTH1

Elena Robeska[1,2], Kévin Lalanne[3], François Vianna[3], Andriy Khobta[4], Didier Busso[5], J. Pablo Radicella[1,2], Anna Campalans[1,2,#], Céline Baldeyron[6,#]

[1] Université Paris Saclay, iRCM/IBFJ, CEA, Genetic Stability, Stem Cells and Radiation, F-92260 Fontenay-aux-Roses, France.

[2] Université de Paris Cité, iRCM/IBFJ, CEA, Genetic Stability, Stem Cells and Radiation, F-92260 Fontenay-aux-Roses, France.

[3] Institut de Radioprotection et de Sûreté Nucléaire (IRSN), PSE-SANTE/SDOS/LMDN, Cadarache, F-13115, Saint-Paul-Lez-Durance, France

[4] Institute of Nutritional Sciences, Friedrich Schiller University Jena, 07743 Jena, Germany.

[5] Université de Paris Cité et Université Paris-Saclay, INSERM, CEA, iRCM/IBFJ, Genetic Stability, Stem Cells and Radiation, F-92260 Fontenay-aux-Roses, France.

[6] Institut de Radioprotection et de Sûreté Nucléaire (IRSN), PSE-SANTE/SERAMED/LRAcc, F-92262 Fontenay aux Roses, France

[*] Corresponding authors: celine.baldeyron@irsn.fr and anna.campalans@cea.fr

Highlights

- Proton microbeam induces, besides DNA double strand breaks (DSB), oxidative base lesions.
- DNA glycosylases OGG1 and NTH1, together with DSB repair proteins, are recruited to the sites of localized proton-irradiation.
- The localization of OGG1 and NTH1 is restricted to the area of damaged DNA, unlike γH2AX.
- The OGG1 and NTH1 release from damaged DNA depends on their enzymatic activity.

Abstract

DNA is the major target of radiation therapy of malignant tumors. Ionizing radiation (IR) induces a variety of DNA lesions, including chemically modified bases and strand breaks. The use of proton beam therapy for cancer treatment is ramping up, as it is expected to reduce normal tissue damage. Thus, it is important to understand the molecular mechanisms of recognition, signaling, and repair of DNA damage induced by protons in the perspective of assessing not only the risk associated with human exposure to IR but also the possibility to

improve the efficacy of therapy. Here, we used targeted irradiation of nuclear regions of living cells with controlled number of protons at a high spatio-temporal resolution to detect the induced base lesions and characterize the recruitment kinetics of the specific DNA glycosylases to DNA damage sites. We show that localized irradiation with 4 MeV protons induces, in addition to DNA double strand breaks (DSBs), the oxidized bases 7,8-dihydro-8-oxoguanine (8-oxoG) and thymine glycol (TG) at the site of irradiation. Consistently, the DNA glycosylases OGG1 and NTH1, capable of excising 8-oxoG and TG, respectively, and initiating the base excision repair (BER) pathway, are recruited to the site of damage. To our knowledge, this is the first direct evidence indicating that proton microbeams induce oxidative base damage, and thus implicating BER in the repair of DNA lesions induced by protons.

Keywords

Proton microbeam; base excision repair; DNA glycosylase; OGG1; NTH1; recruitment kinetics

1. Introduction

DNA is considered a major target for ionizing radiation (IR)-based therapies [1–3]. Exposure of cells to IR has long been known to induce double-strand breaks (DSBs), a particularly cytoxic form of DNA damage [2], but it is only in the mid 1990's that this was visualized *in situ* within the nucleus. Immunofluorescence (IF) detection showed that irradiation of mammalian cells with ^{137}Cs induces the accumulation, into discrete intranuclear foci (also called IRIF for ionizing radiation-induced foci), of RAD51 [4] or RAD50 and MRE11 [5] proteins, all involved in DSB repair (DSBR). These results led to the proposal of the formation of repair centers in response to DNA damage induced by γ-rays. A major advance in the understanding of DNA repair processes of the IR-induced DNA damage arose with the possibility of irradiating subnuclear regions with soft X-rays and monitoring the recruitment of DNA repair proteins by IF [6]. This approach confirmed the hypothesis that proteins involved in the DNA damage response (DDR) [7] are specifically recruited to the irradiated regions, corresponding to DNA damage sites, and opened the door to a wealth of information on the mechanisms underlying the repair of DSBs. More recently, the possibility of inducing localized DNA damage combined with the monitoring of nuclear protein behaviors in living cells by fluorescently tagging them allowed to analyze the kinetics of recruitment of DNA repair factors to IR-induced DSBs [8–10].

Due to its advantages over other IR types, proton beam therapy is increasingly used for the treatment of a variety of cancers [11,12]. Indeed, deposition of the bulk of the beam energy in a defined region, the Bragg peak, allows to minimize its impact on the healthy tissues

found in its path, therefore reducing toxicity [13]. It is therefore important to understand the mechanisms underlying the biological response triggered by such IR. This should allow not only to better assess the risk associated with human exposure but also to identify ways of improving the efficacy of proton therapy. As expected, irradiation with protons also induces DSBs. However, when compared with photon irradiation, at similar doses, irradiation with protons produced larger and more irregularly shaped γH2AX and 53BP1 foci [14–16]. Interestingly, experiments comparing different types of irradiation showed delayed kinetics of repair for some of the lesions generated by protons [14,17], supporting the idea that the DSBs induced by this type of radiation are more often in close proximity with other radiation-induced DNA lesions and therefore more difficult for the cell to repair [18]. While there is an increasingly large literature on the formation and repair of proton-induced DSBs, less is known on what other kinds of lesions are formed at the proximity of DSBs, potentially altering their repair of efficiency. Early work following the localized synthesis of poly(ADP-ribose) after proton beam micro-irradiation [19] suggested the possibility of the induction of single-strand breaks (SSBs), later confirmed experimentally [17]. Generation of clustered lesions, comprising, beside SSBs and DSBs, a mixture of abasic sites and damaged bases, is assumed as well [18]. In particular, the excess of reactive oxygen species (ROS) observed in different cell types upon proton irradiation when compared to photon irradiation [20–22] points to the potential presence of oxidized bases at the site of irradiation. Due to its low oxidative potential, 7,8-dihydro-8-oxoguanine (8-oxoG) is the predominant lesion in DNA exposed to ROS [23,24]. Another oxidized base abundantly formed on DNA following irradiation is thymine glycol (TG) [25–27]. In mammalian cells, 8-oxoG and TG are recognized by specific DNA glycosylases, OGG1 and NTH1, respectively, that initiate the base excision repair (BER) by excising the base and generating an abasic site. The abasic site is then cleaved by APE1 to provide a substrate to a DNA polymerase and a ligase that can then complete the repair process. Other proteins like PARP1 and XRCC1 have also been shown to be involved in both pathways, SSB repair (SSBR) and BER. The use of photon microbeams has allowed the study of the recruitment of DNA glycosylases to laser micro-irradiated regions of cell nuclei [28–32]. However, while there is increasing information on the recruitment of DSBR proteins to the site of DNA damage induced by proton beams [33–35], the formation of other types of lesions and involvement of cognate repair mechanisms has not been explored.

In recent years, microbeam irradiation has been applied as a new approach aimed at deciphering the molecular mechanisms of IR-induced DNA damage recognition, signaling, and repair. Indeed, the ion microbeams provide powerful experimental tools allowing strict control over the site and time of damage and the study of recruitment kinetics of proteins involved in these processes [9,19,36–39]. Here we used the IRSN's MIRCOM facility designed for

targeted irradiation with a focused ion microbeam extracted in air [40] to induce DNA damage by localized proton irradiation within nuclei of living cells with a high spatio-temporal resolution. We show that such a treatment locally induces, in addition to DSBs, 8-oxoG and Tg. Consistently with the formation of oxidative base damage, we detected the recruitment of the DNA glycosylases OGG1 and NTH1, capable of excising 8-oxoG and TG, respectively, and therefore initiating the BER pathway. To our knowledge, this is the first evidence indicating that proton beams induce oxidative DNA damage, and thus involving BER in the repair of DNA lesions induced by protons. Considering the recent developments of BER inhibitors, this observation opens the door to new therapeutical avenues to improve the use of proton therapy.

2. Materials and methods

2.1. Cell lines, culture and transfection

We used Hela cells (German Collection of Microorganisms and Cell Cultures No. ACC 57) to generate NTH1 knock-out cells wherein almost the entire protein-coding sequence was deleted [41]. We transfected HeLa NTH1 KO cells with NTH1-GFP and NTH1(K220Q)-GFP plasmids using Lipofectamine 2000 (Invitrogen, ThermoFisher Scientific) according to the manufacturer's instructions.

U-2 OS cell line (HTB-96, lot 62246950) was obtained from the American Type Culture Collection (ATCC, LGC Standard). We cultured U-2 OS cells in DMEM-GlutaMax medium (Gibco, Life Technologies) supplemented with 10 % (vol/vol) decomplemented fetal calf serum (Eurobio) and 100 U/mL penicillin and 100 µg/mL streptomycin (Gibco, Life Technologies) in a humidified atmosphere with 5 % CO_2 at 37 °C. We transfected 30,000 U-2 OS cells by 0.1 µg of plasmid with TurboFect (ThermoFisher Scientific). We performed transfections in suspension according to the manufacturer's instructions and immediately plated the cells on 4 µm thick polypropylene foil (Goodfellow) previously coated with Cell-Tak (2 µg/cm^2, Corning, Fisher Scientific) on specific PEEK dishes, described in [42]. After plating, we kept cells in a humidified atmosphere with 5 % CO_2 at 37 °C and performed localized irradiation 24-48 h after plasmid transfection.

2.2. Plasmids

The plasmid expressing NTH1(K220Q)-GFP mutated protein was generated from a NTH1-GFP expressing plasmid [29] by site directed mutagenesis using oligonucleotides 5'-TCAGATGGCACACCTGGCTATG-3' (Forward) and 5'–CAGGTGTGCCATCTGAGGCCCAACACCCGGC–3' (Reverse). Plasmids expressing XRCC1-GFP, OGG1-GFP and OGG1(K249Q)-GFP were previously described in [29]. The peGFP+PARP1 plasmid is a kind gift from F. Dantzer (Institut de Recherche de l'Ecole de Biotechnologie de Strasbourg, UMR7242 Biotechnologie et signalisation cellulaire,

Strasbourg, France). The peGFP+53BP1 [43] and peGFP+KU70 [44] constructs were kindly provided by P. Bertrand and by J. Delic (CEA, iRCM/IBFJ, UMRE008 Stabilité Génétique, Cellules Souches et Radiations, Fontenay-aux-Roses, France), respectively.

2.3. Immunoblotting

Cell pellets (from 3 x10^6 cells) were resuspended in 50µL of Lysis buffer (Tris 20 mM, NaCl 20 mM, SDS 0.1%, $MgCl_2$ 1 Mm, Benzonase 0.25 U/µL and Protease inhibitors cocktail 1X) and sonicated for 10 min (with pulses 30 s on / 30 s off). After sonication we centrifuged the samples at 12,000 rpm at 4 °C for 5 min and recovered the supernatants. Protein concentration was measured with the Bradford assay (Bio-Rad), Laemmli buffer was added at a 1x concentration (0.1 % 2-mercaptoethanol, 0.005 % Bromophenol blue, 10 % glycerol, 2 % SDS and 63 mM Tris pH 6.8) before heating for 5 min at 95 °C. We loaded 20 µg of protein extracts in a mini–PROTEAN TGX stain-free gel (Bio-Rad) and used the precision plus protein dual color standards (Bio-Rad) as molecular weight markers. The transfer on nitrocellulose membrane (Bio-Rad) was performed with the Trans-Blot® Turbo™ Transfer System (Bio-Rad). The membrane was blocked for 1 h in blocking solution (PBS-0.1 % Tween 20 containing 3 % milk) and incubated for 1 h at room temperature (RT) with the indicated primary antibodies diluted in blocking solution. Membranes were then washed three times for 5 min with PBS-0.1% Tween20 and further incubated for 45 min at RT with the appropriate secondary antibodies diluted in blocking solution. We imaged Western blots with the Li-Cor Odyssey® DLx imaging system (LI-COR Biosciences).

2.4. DNA glycosylase activity

To measure the NTH1 enzymatic activity in protein extracts obtained from HeLa WT or NTH1-KO cells, previously frozen cells (approx. 5 x10^6 cells) were resuspended in 100 µL of lysis buffer (25 mM Tris pH 7.5, 250 mM NaCl, 1 mM EDTA), sonicated for 10 s (1 s pulses with 10 s intervals, using a Branson digital sonifier, power set to 10%) on ice and centrifuged 90 min at 14,000 rpm and 4 °C. A 34-mer oligonucleotide containing a thymine glycol at position 16 and labeled at the 5' end with Cy5 (5'(Cy5)-GGC TTC ATC GTT GTC (TG)CA GAC CTG GTG GAT ACC G-3') was hybridized to its complementary oligonucleotide containing an adenine opposite the lesion and used as a substrate. We incubated 10 µg of protein extract with 120 fmol of the Cy5-labelled oligonucleotide substrate for one hour at 37 °C in a final volume of 30 µL of reaction buffer (25 mM Tris pH 7.5, 80 mM NaCl, 1 mM EDTA). We stopped the reactions by adding 3 µL of 1.5 M NaOH and incubating further 15 min at 37 °C. We added 8 µL of formamide loading buffer before heating 5 min at 95 °C and loading 20 µl of the reaction in a 20 % polyacrylamide gel containing 7 M urea. We run gels at 400 V for 45 min in 0.5 X TBE running buffer and imaged them using a Typhoon scanner.

2.5. Microbeam irradiation

We performed the irradiation of samples with protons by using the MIRCOM facility, operated by the Institute for Radiological Protection and Nuclear Safety (IRSN) in Cadarache, France. This facility is equipped with a focused ion microbeam line, whose technical details and working principle were previously described in [40]. The beam is produced by a 2 MV Tandetron™ accelerator (HVEE, The Netherlands) that can provide different focused charged particle microbeams, including protons up to 4 MeV. The beam spot size at the sample position, i.e. after in-air extraction, is less than 2.2 ± 0.3 µm (k = 1) [40].

2.5.1. Dose control

The number of ions used for each irradiation was controlled by the definition of an opening time of the microbeam on each target, as described previously [40]. This opening time was calculated by performing periodical ion counting rate measurements with a PIPS (Passivated Implanted Planar Silicon) detector (PD50-12-100AM, Mirion Technologies, France) placed in front of the beam. A mean counting rate can then be obtained and used to define the beam opening time for a given number of ions. In addition, to ensure that the beam did not undergo major fluctuations during the irradiation, we measured the mean counting rate between each sample, and we observed no significant variation of the beam between two consecutive controls, as previously demonstrated in [40]. During the experimental campaigns, for an opening time of 100 ms, we obtained a typical mean number of ions N = 412, with a standard deviation σ = 21 (data not shown), which is close to the expected value from a Poisson law, where $\sigma=\sqrt{N}$.

2.5.2. Irradiation parameters

On the inverted wide-field epifluorescence microscope (AxioObserver™ Z1, Carl Zeiss Microscopy GmbH, Germany) equipped with a 37 °C heating chamber at the end of the MIRCOM beamline, we selected relevant nuclei of GFP-expressing cells with a 20X objective (Zeiss LD Plan-NEOFLUAR 20x/0.4 Korr) through automatic shape recognition by using ImageJ libraries [45] included in a custom-made control software called "MicroIrradiation Application" (MIA)" [40]. We targeted the cells at the center of their nucleus, and we irradiated them with 4 MeV protons using a cross pattern of 5 spots separated by 5 µm (Fig. 1). We thus performed irradiation in a recognizable pattern, to generate DNA damage easily distinguishable from spontaneous DNA damage.

Firstly, to control the targeting accuracy of the microbeam, we used a well characterized GFP-expressing construct, XRCC1-GFP [40,42], to obtain an accurate overlapping between the targeting point (the cross in yellow, Fig. 1A) and the center of the irradiation cross-shaped pattern (the middle dot of the cross of 5 spots in red, Fig. 1). In this case, we delivered 1,000

± 32 protons on each dot. Next, for other GFP-expressing plasmids, we carried out the irradiation by delivering a mean number of 20,000 ± 141 protons on each dot, resulting in a relative fluctuation of 0.7 %. The mean irradiation time was 4.9 s per cell.

2.5.3. Time-lapse imaging

We started time-lapse imaging 10 s before irradiation and recorded images every 2 s with a monochromatic AxioCam™ MRm rev. 3 CCD camera (Carl Zeiss Microscopy GmbH, Germany) using the MIA software. In total, we kept cells in the microbeam chamber for less than 20 min.

2.5.4. Image processing and kinetics analyses

In order to quantify the fluorescence re-localization of GFP-tagged proteins observed with time-lapse imaging, we processed all images using the Fiji software [46]. We selected and followed regions of interest (ROI) manually. We measured the mean intensity of ROIs in every image and plotted them against time. We corrected the resulting data for non-specific fluorescence bleaching and normalized them for the fluorescence intensity measured before irradiation. We analyzed more than 100 spots for each condition from at least 2 independent experiments and performed statistical analyses with Mann-Whitney test.

2.6. Immunofluorescence

2.6.1. Immunostaining

At indicated times following irradiation, we washed the cells twice in PBS (Gibco, Life Technologies) and we performed *in situ* cell fractionation as described previously [47]. Briefly, we rinsed cells with cytoskeleton buffer (CSK) containing 10 mM PIPES pH 6.8, 100 mM NaCl, 300 mM sucrose, 3 mM $MgCl_2$ (Sigma-Aldrich), and a cocktail of protease inhibitors (Complete, EDTA-free tablets, Roche). We immediately performed a Triton X-100 extraction by incubating cells in CSK that contains 0.5 % Triton X-100 (Sigma-Aldrich) for 5 min on ice. After washes with CSK and PBS, we fixed cells with 2 % wt/vol paraformaldehyde (EMS, Euromedex) for 20 min at room temperature (RT). After an additional wash with PBS and two washes with PBT (PBS containing 0.1 % vol/vol Tween 20 (Sigma-Aldrich)), we incubated cells in 5% BSA (Sigma-Aldrich) in PBT for 5 min at RT and subsequently, with the indicated primary antibodies diluted in blocking buffer for overnight incubation at 4 °C. After three washes with PBS and one with blocking buffer, we incubated cells with the appropriate secondary antibodies for 1 h at RT. We washed them three times in PBT, and incubated them with 0.5 µg/mL DAPI (Molecular Probes, Life Technologies) in PBS for 5 min. After three washes in PBS, we mounted samples on polypropylene foil between slide and coverslip in ProLong Diamond mounting medium (Molecular Probes, Life Technologies).

For visualization of 8-oxoG and TG cells were fixed in acetone:methanol (vol:vol) and air dried. We hydrated the cells for 15 min in PBS, and then denatured DNA by incubating cells in 2 N HCl for 45 min at RT. We washed the cells three times in PBS, then neutralized them with 50 mM Tris-HCl pH 8.8 for 5 min and permeabilized them at RT in PB-0.1% Triton for 10 min. We incubated the cells in blocking solution (PBS, 0.1 %Triton, 3 % BSA, 1 % normal goat serum) at 37 °C for 1 h and subsequently for 1 h at 37◦C with the indicated primary antibodies diluted in blocking solution. Then we washed the cells three times for 10 min in PBS-0.1% Triton and incubated them with the appropriate secondary antibodies diluted in blocking solution for 1 h at 37 °C. We counterstained nuclear DNA with DAPI at 1 µg/ml for 5 min.

2.6.2. Image acquisition

We acquired serial z-stack images either on a right confocal LSM780NLO microscope (Carl Zeiss MicroImaging GmbH, Germany), equipped with a Plan-Apochromat 63x/1.4 NA oil M27 objective and piloted with the Zen Black 2011 SP4 software (Carl Zeiss MicroImaging GmbH, Germany) or on a spinning disk microscope (GATACA, W1) using a PlanApo 60x/NA1,4 oil (Nikon, Europe B.V) for visualization of TG and 8-oxoG. We analyzed serial z-stack images by using Fiji software [46]. First, we identified as positive cells those showing a specific staining for the proteins of interest, corresponding to the irradiation pattern drawn, a cross of 5 spots (Fig. 1A). For some images, we carried out profile plot analyses on the image slice with the highest total intensity within cell nuclei to show the localization of DNA repair markers in relation to each other at the same damage spot. The presented data were normalized for the maximum signal intensity.

When necessary, at the indicated time-point post-irradiation, in order to quantify the intensities of GFP inside each individual spot, we performed a sum intensity projection of Z-stacks, selected ROI manually and measured the mean intensity of ROIs in every image for GFP signal and Alexa 594 signal. We corrected obtained data by subtracting the background fluorescence. We presented data of relative GFP intensity normalized for the corrected data of Alexa 594 intensity. We analyzed more than 100 spots for each condition from at least 2 independent experiments and performed statistical analyses with Mann-Whitney test.

2.7. Antibodies

Primary antibodies used during immunoblot (IB) or immunofluorescence (IF) experiments are: mouse anti-H3 (Active Motif MABI 0301, IB: 1:1,000), rabbit anti-Actin (SIGMA A2066; IB, 1:1,000); rabbit anti-GFP (Clontech, Takara Bio Europe SAS, 632592; 1:1,000); mouse anti-γH2AX (Millipore, UpState, 05-636; IF, 1:2,000); rabbit anti-KU70/80 (Abcam, ab 53126; IF, 1:400); rabbit anti-NTH1 (Abcam, ab191413 [EPR15930]; IB, 1:5,000; IF, 1:5,000), mouse anti-TG (JaICA, COGER France, JAI-MTG-100P; IF, 1:2,000); mouse anti-8-oxoG (Abcam, ab62623; IF, 1:2,000).

Secondary antibodies used are: for IB, goat anti-rabbit conjugated to IR800 fluorescent protein or goat anti-mouse conjugated to IR700 fluorescent protein (Advansta Inc., Diagomics, R-05060 and R-05055, respectively; 1:10,000), and for IF, donkey anti-mouse or donkey anti-rabbit coupled to Alexa Fluor 488 or 594 (Invitrogen, ThermoFisher; 1:1,000).

3. Results

3.1. Type of DNA damage detected upon irradiation with microbeam of 4 MeV protons

The microbeam MIRCOM facility allows *in situ* localized 4 MeV proton irradiation within the nuclei of living cells [40]. The MIRCOM microbeam can deliver a controlled number of protons in a specific pattern. In our case we irradiated 5 spots forming a cross so that the irradiated spots in the cell nucleus could be easily visualized (Fig. 1A). The optimization of the system was performed using U-2 OS cells expressing the fusion protein XRCC1-GFP that is very rapidly recruited after induction of SSBs. As previously described [40], XRCC1-GFP readily accumulated at the sites of irradiation (Fig. 1B). Irradiation generally induces a broad spectrum of DNA damage, such as SSB, DSB or base lesions [48]. To investigate what kind of DNA damage is induced upon localized 4 MeV proton irradiation with the MIRCOM microbeam, we assessed the presence of DSBs and base oxidative lesions, such as 8-oxoG and TG. For DSBs, we used an indirect method that consists in revealing their presence by the recruitment to the site of damage of 53BP1 and KU70, both proteins involved in DSB signaling and repair [49]. Proton-irradiated U-2 OS cells transiently expressing GFP-fused 53BP1 or KU70 proteins, displayed a GFP signal showing the expected 5 spots pattern within the cells' nuclei (Fig. 2A). We confirmed the recruitment to the chromatin of the endogenous KU70 in non-transfected cells by immunostaining following Triton X-100 extraction that removes soluble protein pools. We thus observed the presence of KU70/KU80 complex at irradiation sites. We also detected by immunostaining the local enrichment of the specific phosphorylation of the histone variant H2AX (γ-H2AX), as expected in response to DSBs [49–51]. Therefore, our irradiation setting generates DNA damage that leads to recruitment of DDR proteins involved in the cellular response to DSBs.

As previously shown [40,42], GFP fused to XRCC1, a scaffold protein involved in SSBR [52], is recruited to localized proton irradiation-induced DNA damage sites (Figs. 1B and 2B). Since XRCC1 also participates in the BER pathway, and proton irradiation leads to the generation of ROS [20–22], we investigated the formation of oxidized bases at the site of irradiation by using lesion-specific antibodies. We detected within nuclei of U-2 OS cells the induction of oxidative lesions, 8-oxoG and TG, at the site of XRCC1-GFP accumulation following localized irradiation with 4 MeV protons (Fig. 2B).

Taken together, these results demonstrate that with our experimental conditions, the MIRCOM microbeam with 4 MeV protons generates locally within the cell nucleus the major radio-induced DNA lesions, DSBs, oxidized bases and SSBs.

3.2. Recruitment of SSBR and BER proteins to DNA damage sites induced by protons

As PARP1 activity is required for the recruitment of XRCC1 to SSBs [53,54], we verified whether PARP1 also accumulates at the localized irradiation sites, as previously shown by Tartier et al. [19]. We indeed found that in transiently transfected U-2 OS cells PARP1-GFP accumulated at IR-induced DNA damage sites, identified by γ-H2AX staining (Fig. 3A). We also found at these γ-H2AX stained sites the accumulation of XRCC1-GFP (Fig. 3A). PARP1-GFP and XRCC1-GFP dots were located at the center of regions stained by γH2AX (Fig. 3A and C), consistently with the fact that DNA repair proteins, such as PARP1 and XRCC1, are strictly relocated to damaged DNA, surrounded by the γ-H2AX spreading over megabases [55,56]. Reinforcing this hypothesis, XRCC1-GFP, involved both in BER and SSBR, was recruited to the same subnuclear location as the KU complex, involved in DSB repair (Fig. 3A and C).

As our data showed the recruitment of PARP1 and XRCC1 and the formation of oxidized bases at the localized irradiation sites, we next investigated whether the DNA glycosylases initiating BER could be recruited to DNA damage sites induced by a proton microbeam. By overexpressing GFP fusions of the DNA glycosylases NTH1 or OGG1, involved in the repair of TG and 8-oxoG, respectively, we could indeed observe their recruitment to DNA damage sites, where they perfectly colocalized with XRCC1 and with proteins involved in DNA DSBs signaling or repair, such as phosphorylated H2AX or KU complex (Fig. 3B and C). The use of an antibody against NTH1 also allowed the detection of the endogenous DNA glycosylase recruitment and its perfect colocalization with XRCC1-GFP. In addition, we observed that accumulation of NTH1 or OGG1 was also restricted to the center of γ-H2AX marks. Since the DNA glycosylases were detected at the same subnuclear localization, as it was the case for other DNA repair proteins, such as XRCC1 and KU, we conclude that their recruitment was to damaged sites in DNA (Fig. 3B and C).

Therefore, our data show that upon localized irradiation with 4 MeV protons DNA repair proteins from different mechanisms, BER, SSBR and DSBR, are recruited to the same subnuclear irradiated regions.

3.3. DNA glycosylases recruitment kinetics to sites of DNA damage induced by protons are dependent on their catalytic activity.

The kinetics of accumulation of DNA glycosylases at damaged DNA sites were until now mostly analyzed by using laser micro-irradiation [28–32,57]. We thus examined the

dynamic recruitment of OGG1-GFP to DNA damage sites induced by 4 MeV proton irradiation by time-lapse imaging in living cells. Immediately after proton irradiation, OGG1-GFP accumulated at the sites of damage, reaching a maximum level of recruitment within 30 s followed by its gradual release (Fig. 4A and B).

We next investigated whether the accumulation, retention and release of OGG1 at DNA damage sites induced by 4 MeV proton irradiation was modulated by its enzymatic activity. We compared the relative fluorescence intensity at the micro-irradiated sites of wild-type (WT) OGG1-GFP and the mutant OGG1(K249Q)-GFP with an impaired base excision activity but able to bind the lesion [29,58]. Both proteins rapidly accumulated at the irradiated sites and were detected within 5 s upon proton irradiation (Fig. 4B) indicating that the base excision activity of OGG1 is not required for the accumulation of this protein at the site of DNA damage, in agreement with the capacity of the mutant protein to recognize and bind to the 8-oxoG with the same affinity than the WT protein [29,58]. However, the time-lapse imaging shows that the kinetics of OGG1(K249Q)-GFP is distinguishable from the one observed with OGG1-GFP. Indeed, the accumulation of OGG1(K249Q)-GFP to the irradiation site is somewhat delayed in time but, most importantly, is retained at the site of damage much longer than OGG1-GFP (Fig 4B). The fact that the release of OGG1 is impaired in the absence of base excision activity is consistent with previous data [29]. The prolonged retention of OGG1(K249Q)-GFP at damaged DNA was confirmed by immunostaining after CSK extraction, which allows to observe proteins strongly bound to cellular structures, such as chromatin (Fig. 4C). We found that 5 min upon irradiation OGG1(K249Q)-GFP levels were significantly higher compared to the ones measured for OGG1-GFP at the DNA damage sites revealed by KU70/80 staining (Fig. 4C and D).

Having detected the formation of TG, we next investigated whether NTH1, the major DNA glycosylase for the repair of oxidized pyrimidines, was also recruited to the proton-irradiated regions of the nucleus. Indeed, as shown in Fig. 4A, a NTH1-GFP fusion protein was readily recruited to the sites of irradiation. We then asked whether the recruitment of NTH1 *in vivo* to DNA damage sites induced by 4 MeV proton irradiation follows the same dynamic behavior as OGG1. As for OGG1-GFP, we found in transiently transfected U-2 OS cells that NTH1-GFP was rapidly recruited to DNA damage sites following localized proton irradiation (Fig. 5B). NTH1-GFP at the irradiation sites reached a maximum accumulation after 100 s and was gradually released afterwards (Fig. 5B).

In order to evaluate whether the excision activity of NTH1 modulates the dynamic recruitment or release of NTH1 from the damaged region, we generated the mutant protein NTH1(K220Q)-GFP. The mutation of the Lys 220 (named also Lys212 depending on the AUG considered for the initiation of translation) has been shown to be the catalytic active residue of

the enzyme and its mutation to Gln results in an NTH1 protein that can still recognize the lesion but cannot catalyze the excision of the base anymore [59,60]. To confirm the loss of catalytic activity of NTH1(K220Q)-GFP, we transfected either the WT version or the catalytic mutant version of NTH1-GFP plasmid in NTH1 KO Hela cells generated by using CRISPR-Cas9 technology as described in Materials and Methods. The absence of NTH1 expression in the generated clones was validated by WB and IF (Fig. S1). First of all, we confirmed that NTH1-GFP and NTH1(K220Q)-GFP fusion proteins were expressed at similar levels and were stable as they showed an expected size of 65 kDa on Western Blot (Fig. 6A). Next, protein extracts isolated from HeLa cells and NTH1 KO cells overexpressing NTH1-GFP or NTH1(K220Q)-GFP fusion proteins were incubated with an oligonucleotide containing a single TG in order to evaluate their enzymatic activity on the excision of the modified base. The use of this *in vitro* activity assay confirms the loss of the enzymatic activity of the mutant form NTH1(K220Q)-GFP as only the complementation with NTH1-GFP plasmid could rescue the cell extract capacity to process TG in NTH1 KO HeLa cell extracts (Fig. 6, B and C).

We thus decided to investigate the behavior of NTH1(K220Q)-GFP mutant protein upon induction of DNA damage and as we could observe for the OGG1(K249Q) mutant protein, the GFP signal at DNA damage sites persisted for longer time periods compared to the NTH1 WT fusion protein suggesting that the capacity to excise oxidized bases is also required for a rapid release of NTH1 from damaged DNA (Fig. 5, B).

Taken together, our data indicates that irradiation with a proton beam results in the induction of oxidative DNA base modifications 8-oxoG and TG, and as a consequence to the fast recruitment of the DNA glycosylases OGG1 and NTH1 that respectively initiate the repair of those lesions by the BER pathway. The fact that enzymatic activity of the DNA glycosylases is required for their efficient release from the damaged DNA suggests an active repair of the oxidized bases at the site of proton irradiation.

4. Discussion

Our study presents the first evidence that localized proton irradiation induces the oxidatively damaged bases, 8-oxoG and TG, within the cell nucleus. This is consistent with the higher levels of ROS reported upon proton beam irradiation [13,20–22]. By unveiling the presence of a variety of DNA lesions, including SSBs and DSBs as well as oxidized bases, concentrated at the irradiated spots, our results also support the models proposed by proton track simulations by using Monte-Carlo transport codes, which predict the formation of clustered DNA lesions by proton irradiation [61]. High-LET (linear energy transfer) radiation resulting in a high density of ionizing events along the radiation track could induce clusters of lesions that when located within one to two helical turns of the double helix are referred to as

complex DNA damage (CDD). Although the resolution of the imaging systems used here does not allow to determine the proximity of the induced lesions on the double helix, it provides a clear demonstration that BER proteins involved in the repair of base damage and SSBs are indeed recruited to the same nuclear regions as proteins involved in DSBR.

Thus, the variety and complexity of DNA damage induced by proton beams raises the question about the capacity of DNA repair pathways to efficiently perform repair of their cognate lesions in such environment, as well as about the potential interference between them [13,48,62]. Indeed, several studies have shown that while the vast majority of DSB induced by gamma-rays are repaired within 1 hour, they could remain for several days when they are induced in the context of CDD [63].

The difference in kinetics observed between DNA glycosylases OGG1 and NTH1 and their respective active site mutants, suggests that the oxidative base damage induced by the proton microbeam is eventually repaired by the BER. Indeed, the fact that the mutated proteins OGG1(K249Q) and NTH1(K220Q) [60], deficient in their capacity to excise the modified base, remain for longer periods at the site of damage compared to their WT counterparts, strongly suggests that the WT proteins are released from the site of the damage once the modified base is excised. A very fast release of OGG1 from complex DNA damage induced by a pulsed UV laser has also been reported and coincides with the disappearance of the induced 8-oxoG [64]. The release kinetics are in agreement with previous observations showing that the OGG1 mutant OGG1(K249Q) stays associated with the chromatin fraction for longer periods upon induction of the 8-oxoG by chemical methods [58] or by laser micro-irradiation [29,57], when compared to the WT protein. However, more work using heavy ion microbeam will be necessary to establish the spatial and temporal interactions between various damage signaling and repair proteins involved in the IR response and determine if the different pathways implicated interfere with the efficient processing of multiply damaged regions of chromatin following proton irradiation.

It is also important to consider that during the repair of oxidized bases by BER, abasic sites and SSBs are generated as DNA repair intermediates. Considering the high amount and concentration of DNA damage induced by proton beams, these intermediates of BER could potentially be transformed in DSBs as found in the case of ion irradiation [65] and largely contribute to the genomic instability induced by irradiation such as deletions or translocations [66–68]. Furthermore, the retention of BER proteins at the site of irradiation, due either by an impaired catalytic activity or by the presence of neighboring lesions, could also block transcription and/or replication and lead to arrest of cell proliferation or cell death. Interestingly, the overexpression of NTH1 or the inactive mutant NTH1(K220Q) has been shown to induce

genomic instability, micronuclei formation, replicative stress and cellular transformation [60]. The same study showed that overexpression of NTH1 interferes with DSB repair by homologous recombination, one of the two major DSB repair mechanisms [7], independently of its enzymatic activity. Therefore, our results pointing to the formation of CDDs harbouring oxidized pyrimidines, support a model in which both, the generation of DSB that could be induced during the processing by NTH1 of closely induced lesions and the interference of the glycosylase with DSB repair, would contribute to the radiosensitivity observed upon overexpression of NTH1 [69]. This opens some interesting perspectives for hadron cancer therapy. The use of inhibitors against DNA repair proteins PARP and ATM has been shown to sensitize cells to proton irradiation by inducing synthetic lethality [70–73]. Since inhibitors and stimulators of BER proteins have been developed [74–77], and despite some off-target effects recently described [78], those molecules could be used in combination with proton irradiation in order to improve the efficiency for killing cancer cells. In addition, it has been proposed that OGG1 inhibitors affect mostly the proliferation of cancer cells compared to normal cells [79] and could therefore further increase the sensitivity of cancer cells to irradiation while not affecting the normal tissue. The results presented here provide tools to address some of these questions.

5. Conclusion

In conclusion, our data shows for the first time that localized proton irradiation induces the oxidatively damaged bases, 7,8-dihydro-8-oxoguanine and thymine glycol within the cell nucleus. Consequently, the induction of these oxidative DNA base modifications 8-oxoG and TG leads to the fast recruitment of the DNA glycosylases OGG1 and NTH1 that respectively initiate the repair of those lesions by the BER pathway. Finally, the release of OGG1 and NTH1 from the damaged DNA is dependent on their ability to excise the oxidative base lesion.

CRediT authorship contribution statement

Elena Robeska : Investigation; Formal analysis; **Kévin Lalanne :** Investigation; **François Vianna :** Resources; Investigation; **Andriy Khobta :** Resources; Writing - review & editing; **Didier Busso :** Resources; **J. Pablo Radicella :** Conceptualization; Supervision; Funding acquisition; Writing - original draft; Writing - review & editing; **Anna Campalans :** Conceptualization; Supervision; Investigation; Formal analysis; Validation; Visualization; Funding acquisition; Writing - original draft; Writing - review & editing; **Céline Baldeyron :** Conceptualization; Supervision; Investigation; Formal analysis; Validation; Visualization; Funding acquisition; Writing - original draft; Writing - review & editing.

Funding Source

This work was supported by "IRSN-CEA Radiobiologie" program 2019. A.C. and A.K. received founding from the ANR-DFG financial agencies (i.e. Agence nationale de la recherche (ANR, French National Research Agency) [ANR-18-CE92-0013 “TG-TOX” to A.C.] and the Deutsche Forschungsgemeinschaft (DFG, German Research Foundation) [grant number KH263/4 to AK]); the Deutsche Akademische Austausch Dienst (DAAD, German Academic Exchange Service) [grant number 57388935] to A.K. and the Campus France though the collaborative program "Partenariats Hubert Curien (PHC)-PROCOPE" grant to A.C.. E.R. was funded by ANR-18-CE92-0013 “TG-TOX”. K.L. was funded by IRSN Ph.D program.

Declaration of competing interest

The authors declare no conflicts of interest. There was no financial or non-financial assistance provided by a third party for the reported work. There are no patents or copyrights relevant to this work.

Acknowledgements

The authors thank the PSE-SANTE/SDOS/LMDN team of the IRSN for their excellent technical expertise on the MIRCOM facility, Valérie Buard for technical support on the IRSN confocal microscopy facility, and Marta Rodriguez-Alvarez for participation in the validation of the NTH1 knockout cells. We are also grateful to Dr. Stéphane Illiano for his critical reading of the manuscript.

References

[1] D.T. Goodhead, Energy deposition stochastics and track structure: What about the target?, Radiat. Prot. Dosimetry. 122 (2006) 3–15. https://doi.org/10.1093/rpd/ncl498.

[2] D.T. GOODHEAD, J. THACKER, R. COX, Non-rejoining DNA breaks and cell inactivation, Nature. 272 (1978) 379–380. https://doi.org/10.1038/272379a0.

[3] M.A. RITTER, J.E. CLEAVER, C.A. TOBIAS, High-LET radiations induce a large proportion of non-rejoining DNA breaks, Nature. 266 (1977) 653–655. https://doi.org/10.1038/266653a0.

[4] T. Haaf, E.I. Golub, G. Reddy, C.M. Radding, D.C. Ward, Nuclear foci of mammalian Rad51 recombination protein in somatic cells after DNA damage and its localization in synaptonemal complexes, Proc. Natl. Acad. Sci. U. S. A. 92 (1995) 2298–2302. https://doi.org/10.1073/pnas.92.6.2298.

[5] R.S. Maser, K.J. Monsen, B.E. Nelms, J.H. Petrini, hMre11 and hRad50 nuclear foci are induced during the normal cellular response to DNA double-strand breaks, Mol. Cell. Biol. 17 (1997) 6087–6096. https://doi.org/10.1128/mcb.17.10.6087.

[6] B.E. Nelms, R.S. Maser, J.F. MacKay, M.G. Lagally, J.H.J. Petrini, In Situ Visualization of DNA Double-Strand Break Repair in Human Fibroblasts, Science. 280 (1998) 590–592. https://doi.org/10.1126/science.280.5363.590.

[7] S.P. Jackson, J. Bartek, The DNA-damage response in human biology and disease, Nature. 461 (2009) 1071–8. https://doi.org/10.1038/nature08467.

[8] B. Jakob, M. Scholz, G. Taucher-Scholz, Immediate localized CDKN1A (p21) radiation response after damage produced by heavy-ion tracks, Radiat. Res. 154 (2000) 398–405. https://doi.org/10.1667/0033-7587(2000)154[0398:ILCPRR]2.0.CO;2.

[9] B. Jakob, J.H. Rudolph, N. Gueven, M.F. Lavin, G. Taucher-Scholz, Live cell imaging of heavy-ion-induced radiation responses by beamline microscopy, Radiat. Res. 163 (2005) 681–690. https://doi.org/10.1667/RR3374.

[10] J.A. Aten, J. Stap, P.M. Krawczyk, C.H. van Oven, R.A. Hoebe, J. Essers, R. Kanaar, Dynamics of DNA Double-Strand Breaks Revealed by Clustering of Damaged Chromosome Domains, Science. 303 (2004) 92–95. https://doi.org/10.1126/science.1088845.

[11] M. Durante, J.S. Loeffler, Charged particles in radiation oncology, Nat. Rev. Clin. Oncol. 7 (2010) 37–43. https://doi.org/10.1038/nrclinonc.2009.183.

[12] M. Durante, J. Flanz, Charged particle beams to cure cancer: Strengths and challenges, Semin. Oncol. 46 (2019) 219–225. https://doi.org/10.1053/j.seminoncol.2019.07.007.

[13] E.T. Vitti, J.L. Parsons, The radiobiological effects of proton beam therapy: Impact on DNA damage and repair, Cancers (Basel). 11 (2019) 1–15. https://doi.org/10.3390/cancers11070946.

[14] S. Oeck, K. Szymonowicz, G. Wiel, A. Krysztofiak, J. Lambert, B. Koska, G. Iliakis, B. Timmermann, V. Jendrossek, Relating linear energy transfer to the formation and resolution of DNA repair foci after irradiation with equal doses of X-ray photons, plateau, or bragg-peak protons, Int. J. Mol. Sci. 19 (2018). https://doi.org/10.3390/ijms19123779.

[15] A. Gerelchuluun, Z. Hong, L. Sun, K. Suzuki, T. Terunuma, K. Yasuoka, T. Sakae, T. Moritake, K. Tsuboi, Induction of in situ DNA double-strand breaks and apoptosis by

200 MeV protons and 10 MV X-rays in human tumour cell lines, Int. J. Radiat. Biol. 87 (2011) 57–70. https://doi.org/10.3109/09553002.2010.518201.

[16] K. Szymonowicz, A. Krysztofiak, J. van der Linden, A. Kern, S. Deycmar, S. Oeck, A. Squire, B. Koska, J. Hlouschek, M. Vüllings, C. Neander, J.T. Siveke, J. Matschke, M. Pruschy, B. Timmermann, V. Jendrossek, Proton Irradiation Increases the Necessity for Homologous Recombination Repair Along with the Indispensability of Non-Homologous End Joining, Cells. 9 (2020) 889. https://doi.org/10.3390/cells9040889.

[17] R.J. Carter, C.M. Nickson, J.M. Thompson, A. Kacperek, M.A. Hill, J.L. Parsons, Complex DNA Damage Induced by High Linear Energy Transfer Alpha-Particles and Protons Triggers a Specific Cellular DNA Damage Response, Int. J. Radiat. Oncol. 100 (2018) 776–784. https://doi.org/10.1016/j.ijrobp.2017.11.012.

[18] Y. Tokuyama, Y. Furusawa, H. Ide, A. Yasui, H. Terato, Role of isolated and clustered DNA damage and the post-irradiating repair process in the effects of heavy ion beam irradiation, J. Radiat. Res. 56 (2015) 446–455. https://doi.org/10.1093/jrr/rru122.

[19] L. Tartier, C. Spenlehauer, H.C. Newman, M. Folkard, K.M. Prise, B.D. Michael, J. Ménissier-de Murcia, G. de Murcia, Local DNA damage by proton microbeam irradiation induces poly(ADP-ribose) synthesis in mammalian cells, Mutagenesis. 18 (2003) 411–416. https://doi.org/10.1093/mutage/geg015.

[20] X. Zhang, S.H. Lin, B. Fang, M. Gillin, R. Mohan, J.Y. Chang, Therapy-resistant cancer stem cells have differing sensitivity to photon versus proton beam radiation, J. Thorac. Oncol. 8 (2013) 1484–1491. https://doi.org/10.1097/JTO.0b013e3182a5fdcb.

[21] R. Alan Mitteer, Y. Wang, J. Shah, S. Gordon, M. Fager, P.P. Butter, H. Jun Kim, C. Guardiola-Salmeron, A. Carabe-Fernandez, Y. Fan, Proton beam radiation induces DNA damage and cell apoptosis in glioma stem cells through reactive oxygen species, Sci. Rep. 5 (2015) 1–12. https://doi.org/10.1038/srep13961.

[22] E. Giedzinski, R. Rola, J.R. Fike, C.L. Limoli, Efficient Production of Reactive Oxygen Species in Neural Precursor Cells after Exposure to 250 MeV Protons, Radiat. Res. 164 (2005) 540–544. https://doi.org/10.1667/RR3369.1.

[23] S. Kasai, H., Tanooka, H., Nishimura, Formation of 8-hydroxyguanine residues in DNA by X-irradiation, Gan. 75 (1984) 1037–1039. PMID: 6526216.

[24] W.L. Neeley, J.M. Essigmann, Mechanisms of Formation, Genotoxicity, and Mutation of Guanine Oxidation Products, Chem. Res. Toxicol. 19 (2006) 491–505.

https://doi.org/10.1021/tx0600043.

[25] X.C. Le, J.Z. Xing, J. Lee, S.A. Leadon, M. Weinfeld, Inducible repair of thymine glycol detected by an ultrasensitive assay for DNA damage, Science. 280 (1998) 1066–1069. https://doi.org/10.1126/science.280.5366.1066.

[26] J.F. Ward, DNA damage produced by ionizing radiation in mammalian cells: identities, mechanisms of formation, and reparability, Prog. Nucleic Acid Res. Mol. Biol. 35 (1988) 95–125. https://doi.org/10.1016/S0079-6603(08)60611-X.

[27] J.P. Pouget, J.L. Ravanat, T. Douki, M.J. Richard, J. Cadet, Measurement of DNA base damage in cells exposed to low doses of gamma-radiation: comparison between the HPLC-EC and comet assays, Int. J. Radiat. Biol. 75 (1999) 51–58. https://doi.org/10.1080/095530099140807.

[28] L. Lan, S. Nakajima, Y. Oohata, M. Takao, S. Okano, M. Masutani, S.H. Wilson, A. Yasui, In situ analysis of repair processes for oxidative DNA damage in mammalian cells, Proc. Natl. Acad. Sci. 101 (2004) 13738–13743. https://doi.org/10.1073/pnas.0406048101.

[29] A. Campalans, T. Kortulewski, R. Amouroux, H. Menoni, W. Vermeulen, J.P. Radicella, Distinct spatiotemporal patterns and PARP dependence of XRCC1 recruitment to single-strand break and base excision repair, Nucleic Acids Res. 41 (2013) 3115–3129. https://doi.org/10.1093/nar/gkt025.

[30] L. Lan, S. Nakajima, L. Wei, L. Sun, C.-L. Hsieh, R.W. Sobol, M. Bruchez, B. Van Houten, A. Yasui, A.S. Levine, Novel method for site-specific induction of oxidative DNA damage reveals differences in recruitment of repair proteins to heterochromatin and euchromatin, Nucleic Acids Res. 42 (2014) 2330–2345. https://doi.org/10.1093/nar/gkt1233.

[31] H. Menoni, F. Wienholz, A.F. Theil, R.C. Janssens, H. Lans, A. Campalans, J.P. Radicella, J.A. Marteijn, W. Vermeulen, The transcription-coupled DNA repair-initiating protein CSB promotes XRCC1 recruitment to oxidative DNA damage, Nucleic Acids Res. 46 (2018). https://doi.org/10.1093/nar/gky579.

[32] B.M.F. Hanna, M. Michel, T. Helleday, O. Mortusewicz, NEIL1 and NEIL2 are recruited as potential backup for OGG1 upon OGG1 depletion or inhibition by TH5487, Int. J. Mol. Sci. 22 (2021). https://doi.org/10.3390/ijms22094542.

[33] A. Panek, J. Miszczyk, ATM and RAD51 Repair Pathways in Human Lymphocytes

Irradiated with 70 MeV Therapeutic Proton Beam, Radiat. Res. 197 (2022) 396–402. https://doi.org/10.1667/RADE-21-00109.1.

[34] P. Chaudhary, T.I. Marshall, F.J. Currell, A. Kacperek, G. Schettino, K.M. Prise, Variations in the Processing of DNA Double-Strand Breaks Along 60-MeV Therapeutic Proton Beams, Int. J. Radiat. Oncol. 95 (2016) 86–94. https://doi.org/10.1016/j.ijrobp.2015.07.2279.

[35] A.O. Fontana, M.A. Augsburger, N. Grosse, M. Guckenberger, A.J. Lomax, A.A. Sartori, M.N. Pruschy, Differential DNA repair pathway choice in cancer cells after proton- and photon-irradiation, Radiother. Oncol. 116 (2015) 374–380. https://doi.org/10.1016/j.radonc.2015.08.014.

[36] M. Mosconi, U. Giesen, F. Langner, C. Mielke, I. Dalla Rosa, W.G. Dirks, 53BP1 and MDC1 foci formation in HT-1080 cells for low- and high-LET microbeam irradiations, Radiat. Environ. Biophys. 50 (2011) 345–352. https://doi.org/10.1007/s00411-011-0366-9.

[37] N. Uematsu, E. Weterings, K.I. Yano, K. Morotomi-Yano, B. Jakob, G. Taucher-Scholz, P.O. Mari, D.C. Van Gent, B.P.C. Chen, D.J. Chen, Autophosphorylation of DNA-PKCS regulates its dynamics at DNA double-strand breaks, J. Cell Biol. 177 (2007) 219–229. https://doi.org/10.1083/jcb.200608077.

[38] F. Hanton, P. Chaudhary, D. Doria, D. Gwynne, C. Maiorino, C. Scullion, H. Ahmed, T. Marshall, K. Naughton, L. Romagnani, S. Kar, G. Schettino, P. McKenna, S. Botchway, D.R. Symes, P.P. Rajeev, K.M. Prise, M. Borghesi, DNA DSB Repair Dynamics following Irradiation with Laser-Driven Protons at Ultra-High Dose Rates, Sci. Rep. 9 (2019) 4471. https://doi.org/10.1038/s41598-019-40339-6.

[39] V. Hable, G.A. Drexler, T. Brüning, C. Burgdorf, C. Greubel, A. Derer, J. Seel, H. Strickfaden, T. Cremer, A.A. Friedl, G. Dollinger, Recruitment kinetics of DNA repair proteins Mdc1 and Rad52 but not 53BP1 depend on damage complexity, PLoS One. 7 (2012) 1–11. https://doi.org/10.1371/journal.pone.0041943.

[40] F. Vianna, G. Gonon, K. Lalanne, C. Adam-Guillermin, J.F. Bottollier-Depois, L. Daudin, D. Dugué, P. Moretto, M. Petit, L. Serani, J.M. Such, V. Gressier, Characterization of MIRCOM, IRSN's new ion microbeam dedicated to targeted irradiation of living biological samples, Nucl. Instruments Methods Phys. Res. Sect. B Beam Interact. with Mater. Atoms. 515 (2022) 20–30. https://doi.org/10.1016/j.nimb.2022.01.007.

[41] A. Sarmini, Leen; Meabed, Mohammed; Emmanouil, Eirini ; Atsaves, George ; Robeska,

Elena; Karwowski, Bolesław; Campalans, A. Gimisis, Thanasis ; Khobta, Requirement of transcription-coupled nucleotide excision repair for the removal of a specific type of oxidatively induced DNA damage, Nucleic Acids Res. (2023), gkad256, https://doi.org/10.1093/nar/gkad256.

[42] S. Bourret, F. Vianna, G. Devès, V. Atallah, P. Moretto, H. Seznec, P. Barberet, Fluorescence time-lapse imaging of single cells targeted with a focused scanning charged-particle microbeam, Nucl. Instruments Methods Phys. Res. Sect. B Beam Interact. with Mater. Atoms. 325 (2014) 27–34. https://doi.org/10.1016/j.nimb.2014.02.004.

[43] L. Etourneaud, A. Moussa, E. Rass, D. Genet, S. Willaume, C. Chabance-Okumura, P. Wanschoor, J. Picotto, B. Thézé, J. Dépagne, X. Veaute, E. Dizet, D. Busso, A. Barascu, L. Irbah, T. Kortulewski, A. Campalans, C. Le Chalony, S. Zinn-Justin, R. Scully, G. Pennarun, P. Bertrand, Lamin B1 sequesters 53BP1 to control its recruitment to DNA damage, Sci. Adv. 7 (2021) 1–19. https://doi.org/10.1126/sciadv.abb3799.

[44] A. Schellenbauer, M.N. Guilly, R. Grall, R. Le Bars, V. Paget, T. Kortulewski, H. Sutcu, C. Mathé, M. Hullo, D. Biard, F. Leteurtre, V. Barroca, Y. Corre, L. Irbah, E. Rass, B. Theze, P. Bertrand, J.A.A. Demmers, J. Guirouilh-Barbat, B.S. Lopez, S. Chevillard, J. Delic, Phospho-Ku70 induced by DNA damage interacts with RNA Pol II and promotes the formation of phospho-53BP1 foci to ensure optimal cNHEJ, Nucleic Acids Res. 49 (2021) 11728–11745. https://doi.org/10.1093/nar/gkab980.

[45] C.A. Schneider, W.S. Rasband, K.W. Eliceiri, NIH Image to ImageJ: 25 years of image analysis, Nat. Methods. 9 (2012) 671–675. https://doi.org/10.1038/nmeth.2089.

[46] J. Schindelin, I. Arganda-Carrera, E. Frise, K. Verena, L. Mark, P. Tobias, P. Stephan, R. Curtis, S. Stephan, S. Benjamin, T. Jean-Yves, J.W. Daniel, H. Volker, E. Kevin, T. Pavel, C. Albert, Fiji - an Open platform for biological image analysis, Nat. Methods. 9 (2009). https://doi.org/10.1038/nmeth.2019.Fiji.

[47] C. Baldeyron, G. Soria, D. Roche, A.J. Cook, G. Almouzni, HP1alpha recruitment to DNA damage by p150CAF-1 promotes homologous recombination repair, J Cell Biol. 193 (2011) 81–95. https://doi.org/10.1083/jcb.201101030.

[48] M.E. Lomax, L.K. Folkes, P. O'Neill, Biological consequences of radiation-induced DNA damage: Relevance to radiotherapy, Clin. Oncol. 25 (2013) 578–585. https://doi.org/10.1016/j.clon.2013.06.007.

[49] L.H. Thompson, Recognition, signaling, and repair of DNA double-strand breaks

produced by ionizing radiation in mammalian cells: the molecular choreography, Mutat Res Rev Mutat Res. 751 (2012) 158–246. https://doi.org/10.1016/j.mrrev.2012.06.002.

[50] E.P. Rogakou, D.R. Pilch, A.H. Orr, V.S. Ivanova, W.M. Bonner, DNA Double-stranded Breaks Induce Histone H2AX Phosphorylation on Serine 139, J. Biol. Chem. 273 (1998) 5858–5868. https://doi.org/10.1074/jbc.273.10.5858.

[51] E.P. Rogakou, C. Boon, C. Redon, W.M. Bonner, Megabase chromatin domains involved in DNA double-strand breaks in vivo, J. Cell Biol. 146 (1999) 905–915. https://doi.org/10.1083/jcb.146.5.905.

[52] R.E. London, XRCC1 – Strategies for coordinating and assembling a versatile DNA damage response, DNA Repair (Amst). 93 (2020) 102917. https://doi.org/10.1016/j.dnarep.2020.102917.

[53] S. Okano, L. Lan, K.W. Caldecott, T. Mori, A. Yasui, Spatial and Temporal Cellular Responses to Single-Strand Breaks in Human Cells, Mol. Cell. Biol. 23 (2003) 5472–5472. https://doi.org/10.1128/mcb.23.15.5472.2003.

[54] S.F. El-Khamisy, M. Masutani, H. Suzuki, K.W. Caldecott, A requirement for PARP-1 for the assembly or stability of XRCC1 nuclear foci at sites of oxidative DNA damage, Nucleic Acids Res. 31 (2003) 5526–5533. https://doi.org/10.1093/nar/gkg761.

[55] S. Bekker-Jensen, C. Lukas, R. Kitagawa, F. Melander, M.B. Kastan, J. Bartek, J. Lukas, Spatial organization of the mammalian genome surveillance machinery in response to DNA strand breaks, J Cell Biol. 173 (2006) 195–206. https://doi.org/10.1083/jcb.200510130.

[56] L.H. Thompson, T. L.H., L.H. Thompson, Recognition , signaling , and repair of DNA double-strand breaks produced by ionizing radiation in mammalian cells : The molecular choreography, Mutat. Res. - Rev. Mutat. Res. 751 (2012) 158–246. https://doi.org/10.1016/j.mrrev.2012.06.002.

[57] O. D'Augustin, V. Gaudon, C. Siberchicot, R. Smith, C. Chapuis, J. Depagne, X. Veaute, D. Busso, A. Di Guilmi, B. Castaing, J.P. Radicella, A. Campalans, S. Huet, Identification of key residues of the DNA glycosylase OGG1 controlling efficient DNA scanning and recruitment to oxidized bases in living cells, Nucleic Acids Res. (2023), gkad243, https://doi.org/10.1093/nar/gkad243

[58] R. Amouroux, A. Campalans, B. Epe, J.P. Radicella, Oxidative stress triggers the preferential assembly of base excision repair complexes on open chromatin regions,

Nucleic Acids Res. 38 (2010) 2878–2890. https://doi.org/10.1093/nar/gkp1247.

[59] S. Ikeda, T. Biswas, R. Roy, T. Izumi, I. Boldogh, A. Kurosky, A.H. Sarker, S. Seki, S. Mitra, Purification and Characterization of Human NTH1, a Homolog of Escherichia coli Endonuclease III, J. Biol. Chem. 273 (1998) 21585–21593. https://doi.org/10.1074/jbc.273.34.21585.

[60] K.L. Limpose, K.S. Trego, Z. Li, S.W. Leung, A.H. Sarker, J.A. Shah, S.S. Ramalingam, E.M. Werner, W.S. Dynan, P.K. Cooper, A.H. Corbett, P.W. Doetsch, Overexpression of the base excision repair NTHL1 glycosylase causes genomic instability and early cellular hallmarks of cancer, Nucleic Acids Res. 46 (2018) 4515–4532. https://doi.org/10.1093/nar/gky162.

[61] Z. Francis, C. Villagrasa, I. Clairand, Simulation of DNA damage clustering after proton irradiation using an adapted DBSCAN algorithm, Comput. Methods Programs Biomed. 101 (2011) 265–270. https://doi.org/10.1016/j.cmpb.2010.12.012.

[62] L.J. Eccles, P. O'Neill, M.E. Lomax, Delayed repair of radiation induced clustered DNA damage: Friend or foe?, Mutat. Res. - Fundam. Mol. Mech. Mutagen. 711 (2011) 134–141. https://doi.org/10.1016/j.mrfmmm.2010.11.003.

[63] B. Wilkinson, M.A. Hill, J.L. Parsons, The Cellular Response to Complex DNA Damage Induced by Ionising Radiation., Int. J. Mol. Sci. 24 (2023). https://doi.org/10.3390/ijms24054920.

[64] R. Aleksandrov, A. Dotchev, I. Poser, D. Krastev, G. Georgiev, G. Panova, Y. Babukov, G. Danovski, T. Dyankova, L. Hubatsch, A. Ivanova, A. Atemin, M.N. Nedelcheva-Veleva, S. Hasse, M. Sarov, F. Buchholz, A.A. Hyman, S.W. Grill, S.S. Stoynov, Protein Dynamics in Complex DNA Lesions, Mol. Cell. 69 (2018) 1046-1061.e5. https://doi.org/10.1016/j.molcel.2018.02.016.

[65] B. Jakob, M. Dubiak-Szepietowska, E. Janiel, A. Schmidt, M. Durante, G. Taucher-Scholz, Differential Repair Protein Recruitment at Sites of Clustered and Isolated DNA Double-Strand Breaks Produced by High-Energy Heavy Ions, Sci. Rep. 10 (2020) 1443. https://doi.org/10.1038/s41598-020-58084-6.

[66] J.M. Danforth, L. Provencher, A.A. Goodarzi, Chromatin and the cellular response to particle radiation-induced oxidative and clustered DNA damage, Front. Cell Dev. Biol. 10 (2022) 1–24. https://doi.org/10.3389/fcell.2022.910440.

[67] G. Iliakis, E. Mladenov, V. Mladenova, Necessities in the Processing of DNA Double

Strand Breaks and Their Effects on Genomic Instability and Cancer, Cancers (Basel). 11 (2019) 1671. https://doi.org/10.3390/cancers11111671.

[68] M.P. Souli, Z. Nikitaki, M. Puchalska, K.P. Brabcová, E. Spyratou, P. Kote, E.P. Efstathopoulos, M. Hada, A.G. Georgakilas, L. Sihver, Clustered DNA Damage Patterns after Proton Therapy Beam Irradiation Using Plasmid DNA, Int. J. Mol. Sci. 23 (2022). https://doi.org/10.3390/ijms232415606.

[69] N. Yang, H. Galick, S.S. Wallace, Attempted base excision repair of ionizing radiation damage in human lymphoblastoid cells produces lethal and mutagenic double strand breaks, DNA Repair (Amst). 3 (2004) 1323–1334. https://doi.org/10.1016/j.dnarep.2004.04.014.

[70] C. Zhou, M.R. Fabbrizi, J.R. Hughes, G.J. Grundy, J.L. Parsons, Effectiveness of PARP inhibition in enhancing the radiosensitivity of 3D spheroids of head and neck squamous cell carcinoma, Front. Oncol. 12 (2022) 1–15. https://doi.org/10.3389/fonc.2022.940377.

[71] L. Wang, J. Cao, X. Wang, E. Lin, Z. Wang, Y. Li, Y. Li, M. Chen, X. Wang, B. Jiang, R. Zhang, N. Sahoo, X. Zhang, X.R. Zhu, J.N. Myers, S.J. Frank, Proton and photon radiosensitization effects of niraparib, a PARP-1/-2 inhibitor, on human head and neck cancer cells, Head Neck. 42 (2020) 2244–2256. https://doi.org/10.1002/hed.26155.

[72] E.T. Vitti, A. Kacperek, J.L. Parsons, Targeting DNA Double-Strand Break Repair HPV-Negative Head and Neck Squamous Cell, Cancers (Basel). 12 (2020) 1490. https://doi.org/10.3390/cancers12061490.

[73] Q. Zhou, M.E. Howard, X. Tu, Q. Zhu, J.M. Denbeigh, N.B. Remmes, M.G. Herman, C.J. Beltran, J. Yuan, P.T. Greipp, J.C. Boughey, L. Wang, N. Johnson, M.P. Goetz, J.N. Sarkaria, Z. Lou, R.W. Mutter, Inhibition of ATM induces hypersensitivity to proton irradiation by upregulating toxic end joining, Cancer Res. 81 (2021) 3333–3346. https://doi.org/10.1158/0008-5472.CAN-20-2960.

[74] Y. Tahara, D. Auld, D. Ji, A.A. Beharry, A.M. Kietrys, D.L. Wilson, M. Jimenez, D. King, Z. Nguyen, E.T. Kool, Potent and Selective Inhibitors of 8-Oxoguanine DNA Glycosylase, J. Am. Chem. Soc. 140 (2018) 2105–2114. https://doi.org/10.1021/jacs.7b09316.

[75] T. Visnes, M. Grube, B.M.F. Hanna, C. Benitez-Buelga, A. Cázares-Körner, T. Helleday, Targeting BER enzymes in cancer therapy, DNA Repair (Amst). 71 (2018) 118–126. https://doi.org/10.1016/j.dnarep.2018.08.015.

[76] M. Michel, C. Benítez-Buelga, P.A. Calvo, B.M.F. Hanna, O. Mortusewicz, G. Masuyer, J. Davies, O. Wallner, K. Sanjiv, J.J. Albers, S. Castañeda-Zegarra, A.S. Jemth, T. Visnes, A. Sastre-Perona, A.N. Danda, E.J. Homan, K. Marimuthu, Z. Zhenjun, C.N. Chi, A. Sarno, E. Wiita, C. von Nicolai, A.J. Komor, V. Rajagopal, S. Müller, E.C. Hank, M. Varga, E.R. Scaletti, M. Pandey, S. Karsten, H. Haslene-Hox, S. Loevenich, P. Marttila, A. Rasti, K. Mamonov, F. Ortis, F. Schömberg, O. Loseva, J. Stewart, N. D'Arcy-Evans, T. Koolmeister, M. Henriksson, D. Michel, A. de Ory, L. Acero, O. Calvete, M. Scobie, C. Hertweck, I. Vilotijevic, C. Kalderén, A. Osorio, R. Perona, A. Stolz, P. Stenmark, U.W. Berglund, M. de Vega, T. Helleday, Small-molecule activation of OGG1 increases oxidative DNA damage repair by gaining a new function, Science. 376 (2022) 1471–1476. https://doi.org/10.1126/science.abf8980.

[77] N. Donley, P. Jaruga, E. Coskun, M. Dizdaroglu, A.K. McCullough, R.S. Lloyd, Small Molecule Inhibitors of 8-Oxoguanine DNA Glycosylase-1 (OGG1), ACS Chem. Biol. 10 (2015) 2334–2343. https://doi.org/10.1021/acschembio.5b00452.

[78] X. Tanushi, G. Pinna, M. Vandamme, C. Siberchicot, O. D'Augustin, A.M. Di Guilmi, J.P. Radicella, B. Castaing, R. Smith, S. Huet, F. Leteurtre, A. Campalans, OGG1 competitive inhibitors show important off-target effects by directly inhibiting efflux pumps and disturbing mitotic progression, Front. Cell Dev. Biol. 11 (2023) 1–15. https://doi.org/10.3389/fcell.2023.1124960.

[79] T. Visnes, C. Benítez-Buelga, A. Cázares-Körner, K. Sanjiv, B.M.F. Hanna, O. Mortusewicz, V. Rajagopal, J.J. Albers, D.W. Hagey, T. Bekkhus, S. Eshtad, J.M. Baquero, G. Masuyer, O. Wallner, S. Müller, T. Pham, C. Göktürk, A. Rasti, S. Suman, R. Torres-Ruiz, A. Sarno, E. Wiita, E.J. Homan, S. Karsten, K. Marimuthu, M. Michel, T. Koolmeister, M. Scobie, O. Loseva, I. Almlöf, J.E. Unterlass, A. Pettke, J. Boström, M. Pandey, H. Gad, P. Herr, A.S. Jemth, S. El Andaloussi, C. Kalderén, S. Rodriguez-Perales, J. Benítez, H.E. Krokan, M. Altun, P. Stenmark, U.W. Berglund, T. Helleday, Targeting OGG1 arrests cancer cell proliferation by inducing replication stress, Nucleic Acids Res. 48 (2021) 12234–12251. https://doi.org/10.1093/nar/gkaa1048.

Figure Legends

Fig. 1. Targeted irradiation with 4 MeV protons on the MIRCOM facility. (A) *Experimental scheme for targeted irradiation with 4 MeV protons in a cross pattern of 5 spots.* After transfection, we selected cell nuclei and irradiated them in a cross pattern of 5 spots separated

by 5 µm from each other. For the irradiation, we delivered a mean number of 20,000 ± 141 protons on each spot, resulting in a relative fluctuation of 0.7 %. Immediately after, either we performed live cell imaging and monitored the behavior of GFP-tagged proteins at local irradiation sites, or we carried out immunostaining of irradiated cells. **(B)** *Real-time accumulation of XRCC1-GFP protein within cell nucleus upon localized irradiation with 4 MeV protons.* We transiently transfected U-2 OS cells with a plasmid coding for a GFP fused to XRCC1. A day after, we targeted the center of nuclei of GFP-positive cells (yellow cross) and irradiated according to a 10 µm-wide cross pattern of 5 points (red cross of 5 spots) defined as in Fig. 1B. We delivered at each point 1,000 ± 32 protons. The irradiation started at 0 s. Scale bar represents 10 µm.

Fig. 2. DNA lesions induced by a microbeam irradiation with protons in U-2 OS cells. (A) *Indirect detection of DNA double-strand breaks (DSBs) at localized irradiation sites.* We transiently transfected U-2 OS cells with peGFP plasmid coding for proteins involved in DSB repair mechanisms, such as 53BP1 or KU70. A day after, we locally irradiated nuclei of cells expressing GFP-tagged proteins by using the pattern described in Fig. 1B and we delivered at each point 20,000 ± 141 protons. At the indicated time, we permeabilized cells with CSK + Triton X-100 to remove soluble nuclear components and fixed them. We performed immunostaining with either an anti-KU70/80 or an anti-γH2AX antibody and visualized GFP-tagged proteins. **(B)** *Direct detection of oxidative base damage at localized irradiation sites.* We irradiated U-2 OS cells transiently transfected with peGFP+XRCC1 plasmid as in (A). At the indicated time, we fixed cells by acetone:methanol and carried out a DNA denaturation uncovering oxidative lesions. We then performed immunostaining with either an anti-TG antibody or an anti-8-oxoG antibody in addition to an anti-GFP antibody for visualizing XRCC1-GFP. For each immunostaining (A and B), we showed a representative cell from unirradiated cell pool (untargeted) and proton microbeam irradiated cell pool (targeted) on the same dish. DNA is stained with DAPI. Bars, 10 µm.

Fig. 3. Recruitment of BER proteins to localized proton irradiation sites. (A) *Recruitment of BER proteins involved in the repair of DNA strand breaks***.** We transiently transfected U-2 OS cells with plasmid expressing GFP fused either to PARP1 or XRCC1. We treated transfected cells as in Fig. 2A. At the indicated time, after Triton extraction and fixation, we performed immunostaining with either an anti-γH2AX or an anti-KU70/80 antibody and visualized GFP-tagged proteins**. (B)** *Recruitment of BER proteins involved in the repair of base lesions***.** We transiently transfected U-2 OS cells with plasmid expressing GFP fused either to XRCC1 or to DNA glycosylases, such as NTH1 or OGG1. We treated transfected cells as in Fig. 2A. At the indicated time, after Triton extraction and fixation, we performed immunostaining with either an anti-NTH1 or an anti-KU70/80 antibody and visualized GFP-tagged proteins**.**

DNA is stained with DAPI. Bars, 10 µm. **(C)** *Spatial occupancy of DNA repair proteins at irradiated regions.* We displayed the intensity profiles corresponding to the white lines in each enlarged merge view from (A, B), which go through an individual irradiated spot. The enlarged views are a zoom of the dotted white boxed regions from (A, B). The profile plots show the intensity measurements in arbitrary units (a.u.) from GFP-tagged proteins (green lines) and proteins revealed by immunostaining (i.e., γH2AX, KU70/80 or NTH1, red lines). The presented data are normalized to the maximum of the intensity of each signal.

Fig. 4. Recruitment kinetics of OGG1 to localized proton irradiation sites. (A) *Recruitment of OGG1 upon proton irradiation.* To analyze the behavior of OGG1 after proton irradiation, we irradiated as in Fig. 2A U-2 OS cells expressing GFP-fused OGG1 wild-type or carrying the K249Q mutation. Immediately after, we performed live cell imaging on an epifluorescent Zeiss microscope and monitored the behavior of GFP-tagged proteins at the targeted irradiation spots. **(B)** *Dynamic behavior of OGG1 upon proton irradiation.* Graph corresponds to mean values from at least 100 spots within nuclei of cells irradiated in (A). The irradiation was applied at t = 10 s. We show the standard error of the mean (SEM) by error bars and the p values from Mann-Whitney test by asterisks (*** $p < 0.001$). **(C)** *Localization of OGG1 at the localized proton irradiation.* At the indicated time after irradiation, we permeabilized cells irradiated in (A) and fixed them. We then performed immunostaining with an anti-KU70/80 and visualized OGG1 proteins, wild-type and mutant, by the direct detection of GFP signal. DNA is stained with DAPI. Bars, 10 µm. **(D)** *Level of OGG1-GFP and OGG1(K249Q)-GFP proteins at irradiated DNA.* We measured the GFP signals at irradiation (IR) spots from (C). The data shown in scatter dot plots represent the background corrected fluorescence intensities corresponding to GFP-OGG1 or OGG1(K249Q)-GFP normalized by the background corrected fluorescence intensities corresponding to the immunostaining signal of KU70/80. Bold bars represent the mean, error bars the standard error of the mean (SEM) and asterisks the p values from Mann-Whitney test (***$p < 0.001$).

Fig. 5. Recruitment kinetics of NTH1 to localized proton irradiation sites. (A) *Recruitment of NTH1 upon proton irradiation.* To analyze the behavior of NTH1 after proton irradiation, we irradiated as in Fig. 2A U-2 OS cells expressing GFP-fused NTH1 wild-type or carrying the K220Q mutation. Immediately after, we performed live cell imaging on an epifluorescent Zeiss microscope and monitored the behavior of GFP-tagged proteins at the targeted irradiation spots. Bars, 10 µm. **(B)** *Dynamic behavior of NTH1 upon proton irradiation.* Graph corresponds to mean values from at least 100 spots within cells irradiated in (A). Error bars represent SEM. The irradiation occured at t = 10 s. Statistical test was performed with Mann-Whitney test and ** $p < 0.01$.

Fig. 6. Complementation of NTH1 knock-out cells generated by CRISPR-Cas9 with NTH1-WT and the inactive mutant NTH1(K220Q) fused to the GFP. (A) *Expression of NTH1-GFP proteins.* Western-Blots performed from protein extracts were analyzed using an antibody against NTH1 allowing to visualize both the endogenous NTH1 (indicated with an *) and the overexpressed NTH1-GFP fusion proteins. H3 was used as a loading control. **(B)** *Enzymatic activity of NTH1-GFP proteins.* Protein extracts from WT, KO, and KO cells complemented with WT NTH1-GFP and the mutant NTH1(K220Q)-GFP were analyzed for their capacity to process TG. *In vitro* enzymatic activity was performed using an oligonucleotide containing one single TG. **(C)** Quantification of cleavage products. Graph represents the mean $^{+}$/- SD from three independent experiments.

Robeska et al., Graphical abstract

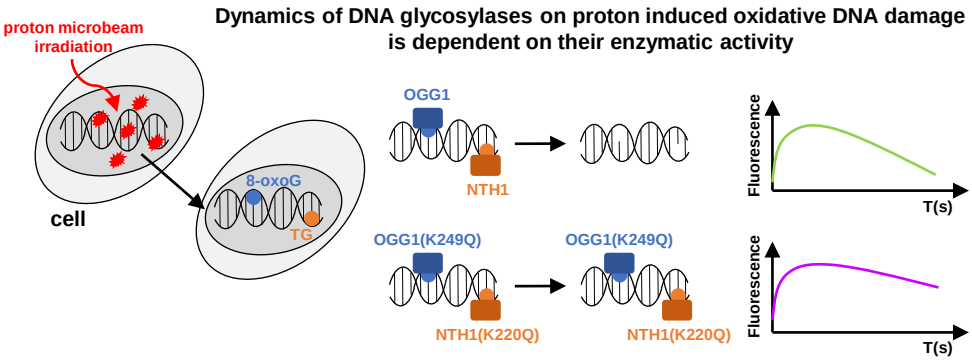

Robeska et al., Figure 1 *(a 2-column fitting image)*

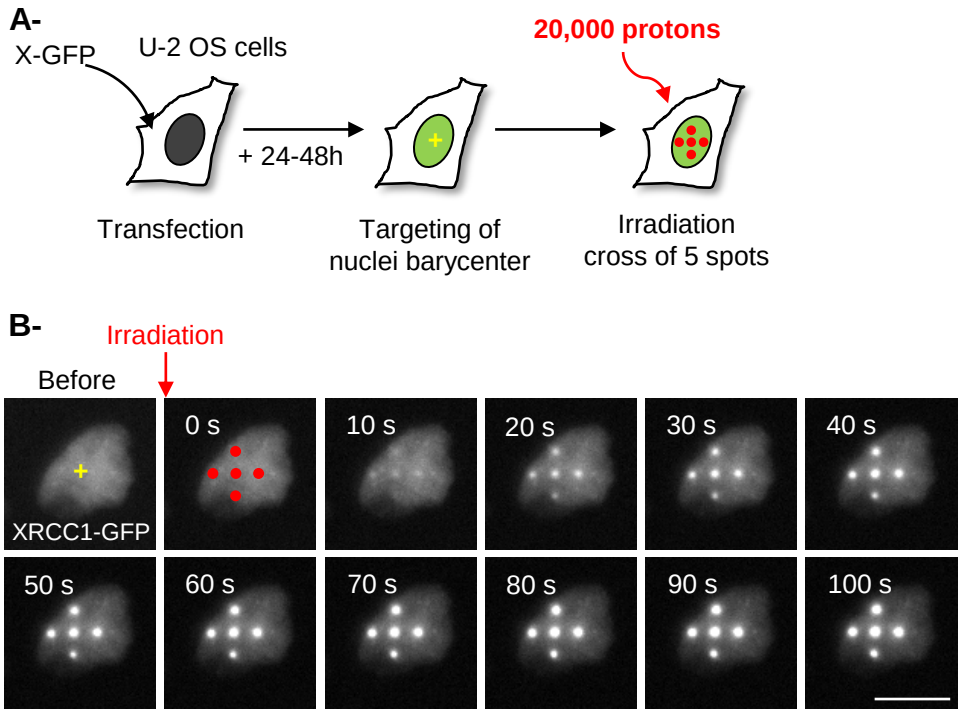

Robeska et al., Figure 2 *(a 1.5-column fitting image)*

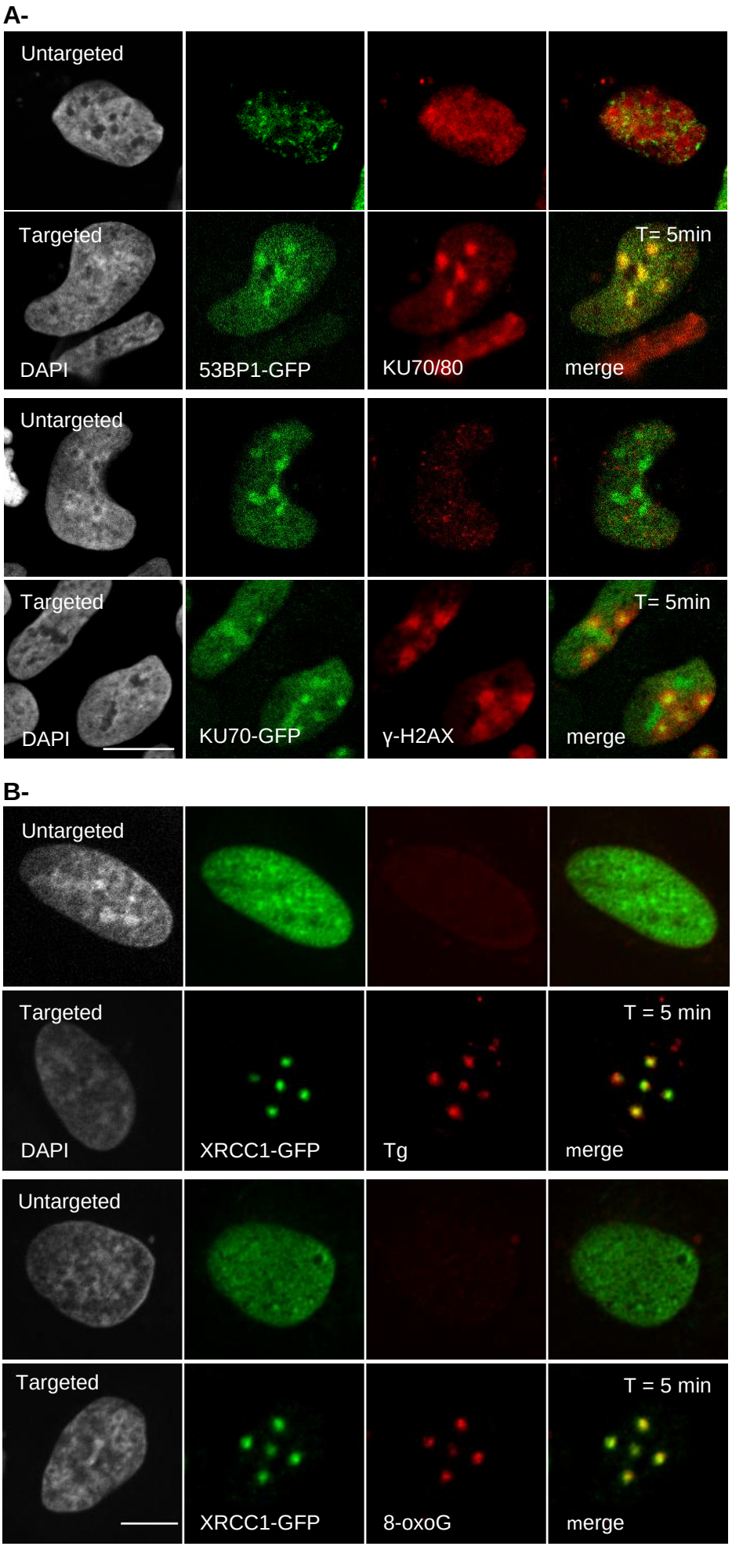

Robeska et al., Figure 3 *(a 2-column fitting image)*

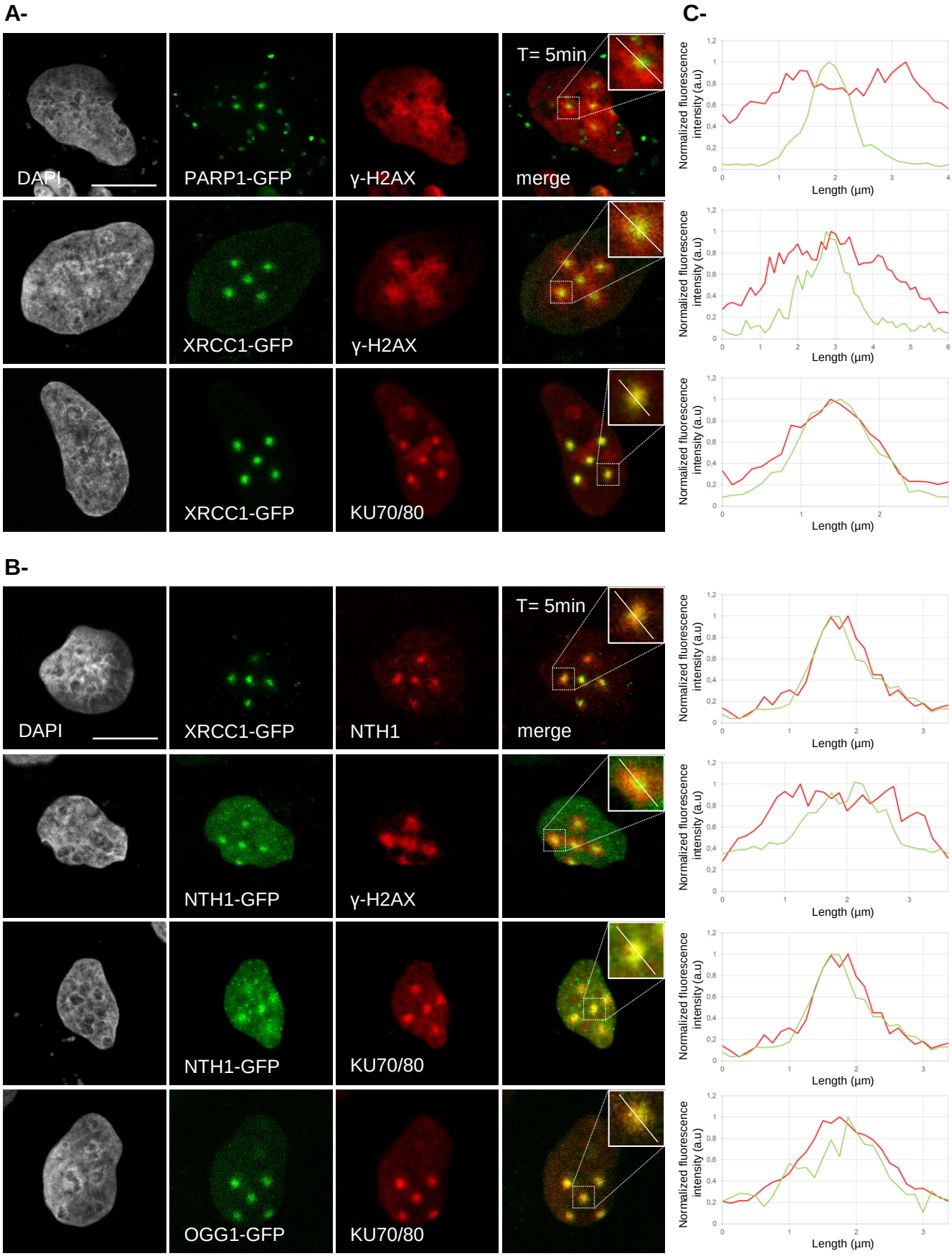

Robeska et al., Figure 4 *(a 2-column fitting image)*

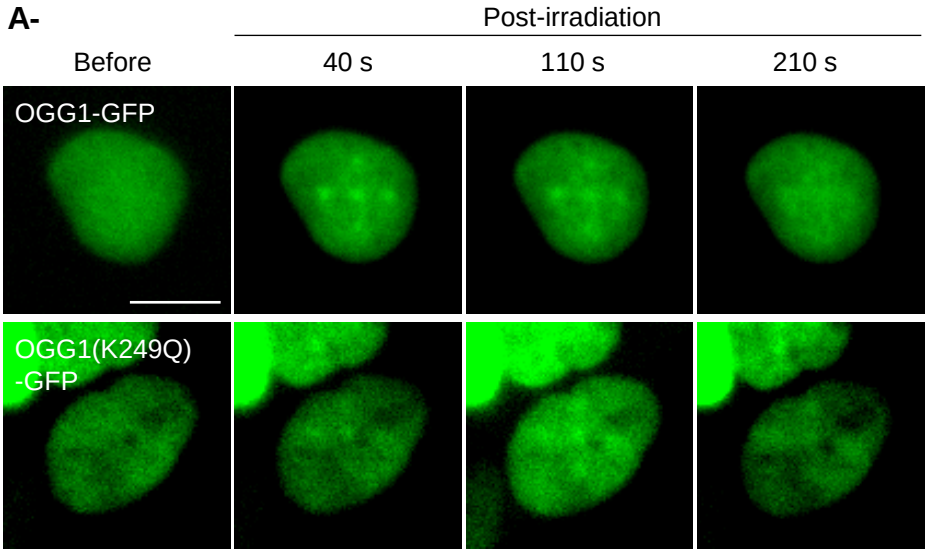

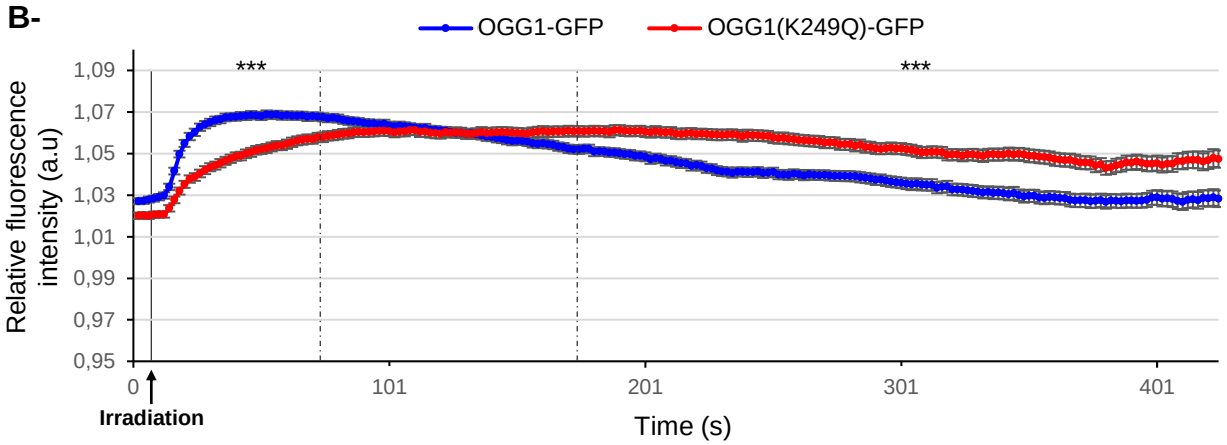

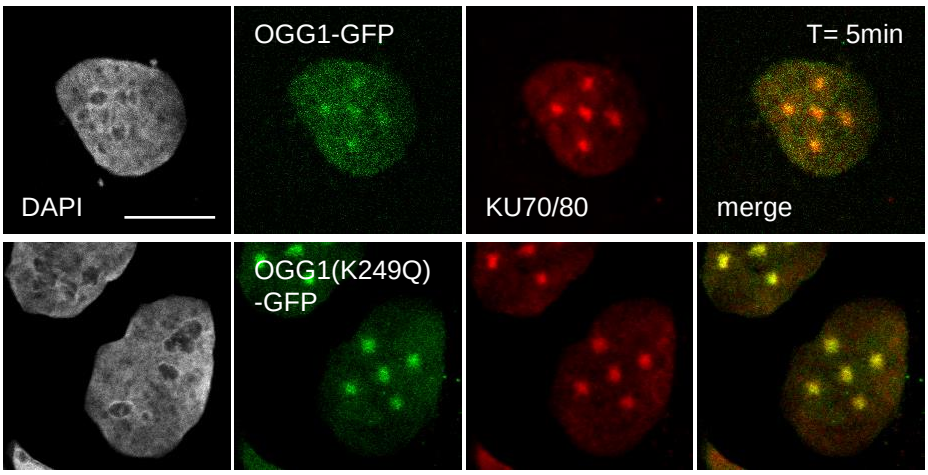

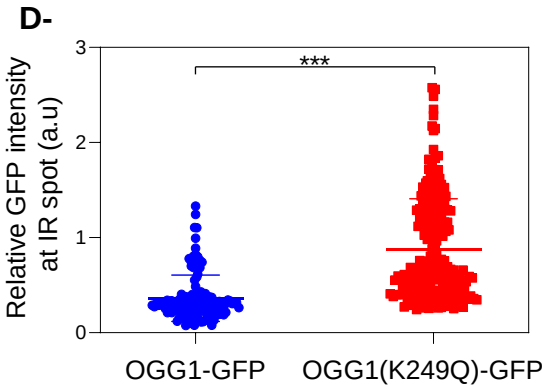

Robeska et al., Figure 5 *(a 2-column fitting image)*

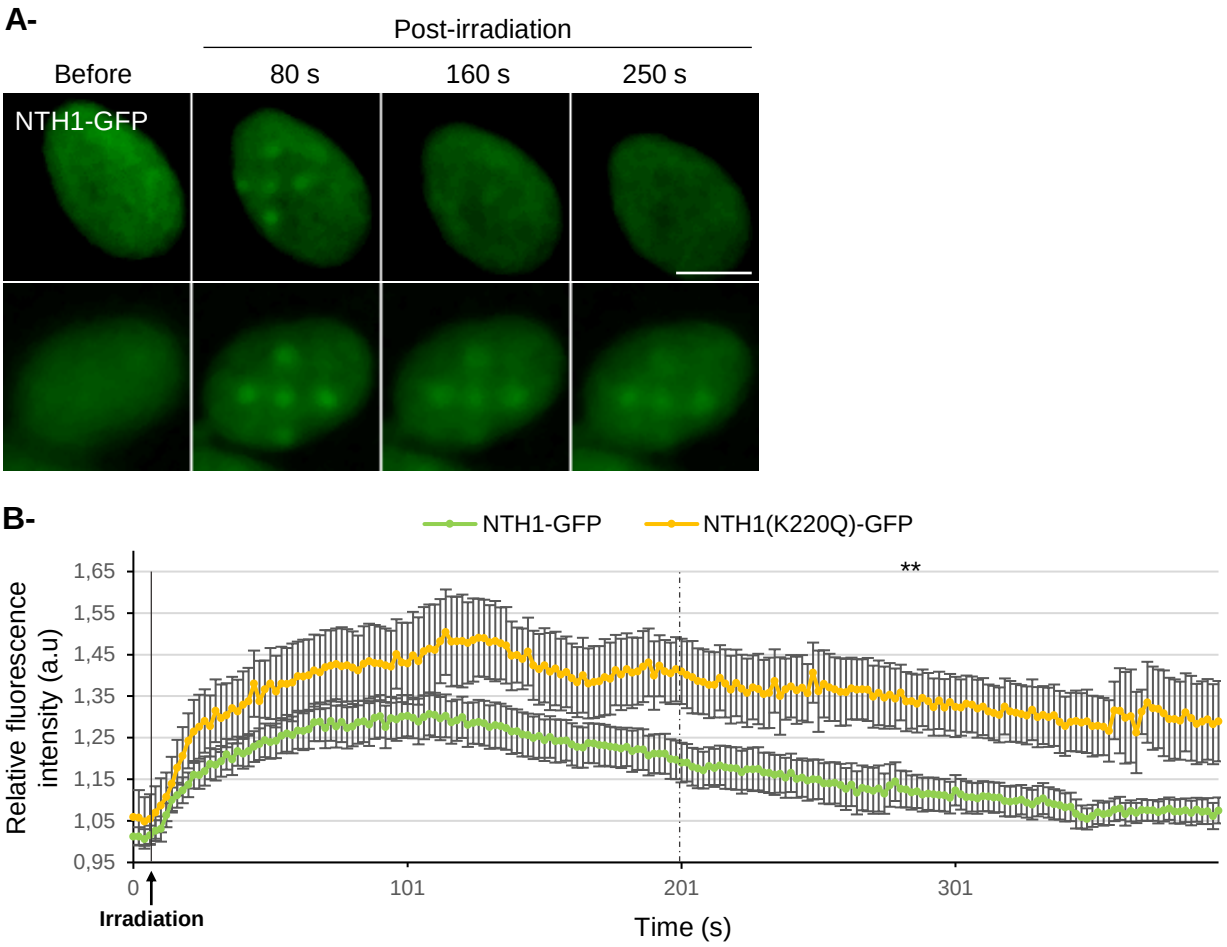

Robeska et al., Figure 6 *(a 1.5-column fitting image)*

A-

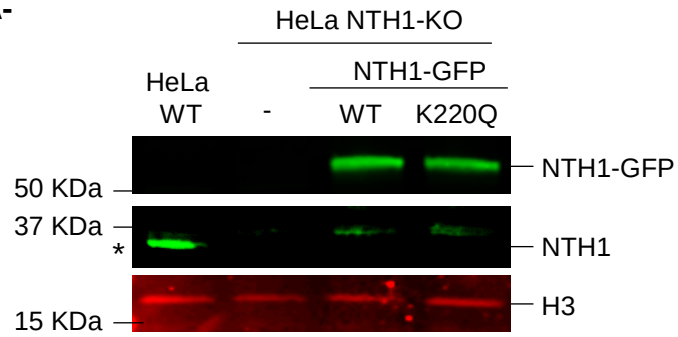

B-

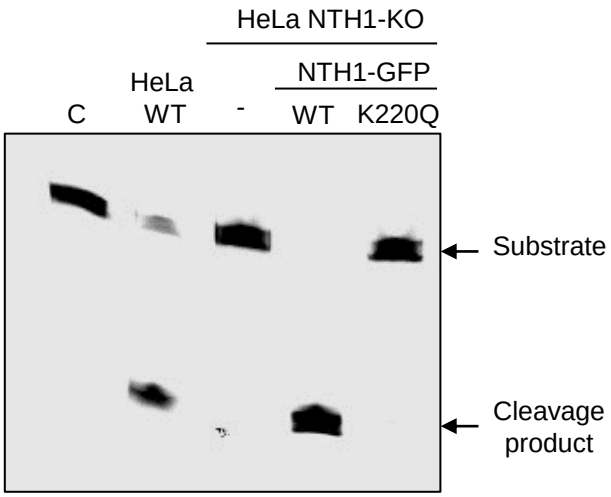

C-

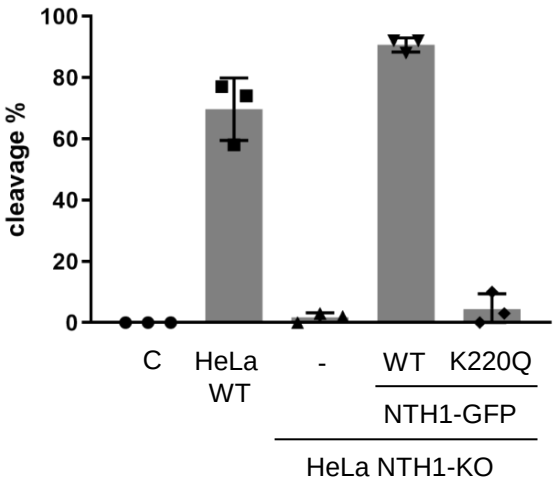

Robeska et al., Figure S1 *(a 1.5-column fitting image)*

A-

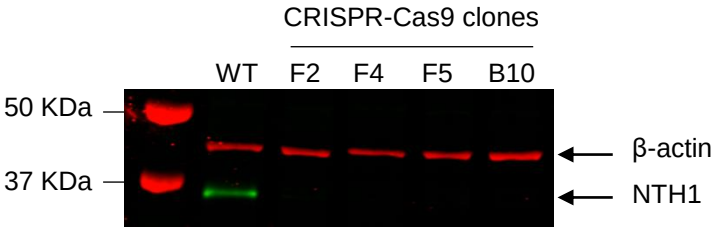

B-